

Quantum Inflation: A General Approach to Quantum Causal Compatibility

Elie Wolfe,¹ Alejandro Pozas-Kerstjens,^{2,3} Matan Grinberg,⁴
Denis Rosset,⁵ Antonio Acín,^{3,6} and Miguel Navascués⁷

¹*Perimeter Institute for Theoretical Physics, N2L 2Y5 Waterloo, Canada*

²*Departamento de Análisis Matemático, Universidad Complutense de Madrid, 28040 Madrid, Spain*

³*ICFO-Institut de Ciencies Fotoniques, The Barcelona Institute of Science and Technology, 08860 Castelldefels (Barcelona), Spain*

⁴*Princeton University, Princeton, NJ USA 08544*

⁵*Perimeter Institute for Theoretical Physics, Waterloo, Ontario, Canada, N2L 2Y5*

⁶*ICREA, Passeig Lluís Companys 23, 08010 Barcelona, Spain*

⁷*Institute for Quantum Optics and Quantum Information (IQOQI), Boltzmanngasse 3 1090 Vienna, Austria*

Causality is a seminal concept in science: any research discipline, from sociology and medicine to physics and chemistry, aims at understanding the causes that could explain the correlations observed among some measured variables. While several methods exist to characterize classical causal models, no general construction is known for the quantum case. In this work we present quantum inflation, a systematic technique to falsify if a given quantum causal model is compatible with some observed correlations. We demonstrate the power of the technique by reproducing known results and solving open problems for some paradigmatic examples of causal networks. Our results may find an application in many fields: from the characterization of correlations in quantum networks to the study of quantum effects in thermodynamic and biological processes.

I. INTRODUCTION

Causality is an ubiquitous concept in science. It can be argued that one of the main challenges in any scientific discipline is to identify which causes are behind the correlations observed among some measured variables, encapsulated by their joint probability distribution. Understanding this problem is crucial in many situations, such as, for example, the development of medical treatments, taking data-based social policy decisions, the design of new materials or the theoretical modeling of experiments. More precise characterizations of causal correlations enable better decision among competing explanations for given statistics, a task known as **causal discovery**. Advances in causal understanding also enables quantification of causal effects from purely observational data, thus extracting counterfactual conclusions even in instances where randomized or controlled trials are not feasible, a task known as **causal inference** [1–3].

Bayesian causal networks, in the form of directed acyclic graphs (DAGs), provide the tools to formalise such problems. These graphs, examples of which are shown in Fig. 1, encode the causal relations between the various variables in the problem, which could be either observed or non-observed. The latter, also known as latent, are required in many relevant situations in order to explain correlations among the observed. The fundamental task addressed in this work underlies both causal discovery and causal inference, and is known as the **causal compatibility** problem. It consists of deciding whether a given joint probability distribution over some observed variables can be explained by a given candidate Bayesian causal network. Equivalently, the objective of causal compatibility can be viewed as characterizing the set of distributions compatible with

a given Bayesian network.

In all cases, the measured variables in a causal network are, by definition, classical. However, causal networks may be classical or quantum depending on whether correlations are established by means of classical or quantum information. Because of its importance and broad range of applications, there is a vast literature devoted to understanding the problem of causal compatibility for classical causal networks, see for instance Ref. [1]. On the contrary, very little is known for the quantum case despite the fact that nature is ultimately quantum and quantum effects are expected to be crucial for the understanding of many relevant phenomena in many scientific disciplines. Moreover the two problems are known to be different, as one of the consequences of Bell’s theorem [4, 5] is that quantum causal networks can explain correlations for which the analogous classical network fails [6–10]. Our work addresses these issues and provides a systematic construction to tackle the problem of causal compatibility for quantum causal networks.

As mentioned, several results already exist in the classical case. Whenever the network does not contain any latent variable the solution is rather simple and it suffices to check whether all the conditional independences associated to the network topology are satisfied [1]. The problem, however, becomes much more difficult as soon as the network also includes latent variables, as their presence generally implies non-trivial inequalities on the observed probabilities. A general method to tackle the causal compatibility problem, known as the **inflation technique**, was obtained in [11]. It consists of a hierarchy of conditions, organised according to their computational cost, that are necessary for a Bayesian network to be able to explain the observed correlations. Moreover, the hierarchy is asymptotically sufficient, in the sense that

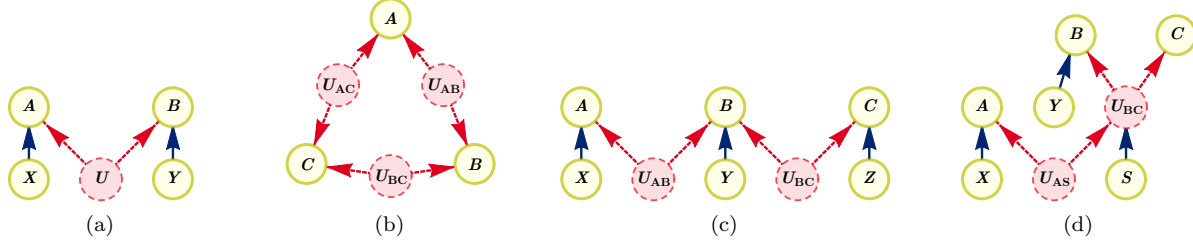


FIG. 1. DAG representation of different causal scenarios. The red, dashed circles are latent variables, and the yellow, single-lined circles denote visible variables. (a) The Bell scenario is one of the simplest causal structures exhibiting a classical-quantum gap, that is, where there exist distributions that can be realized with quantum latent variables (denoted as $U=\rho$), but not with classical ones (denoted as $U=\lambda$). (b) The triangle scenario also presents a classical-quantum gap. Alternatively, the triangle scenario can also be defined with one visible variable (called *measurement choice*) influencing each of A , B and C . (c) The tripartite-line causal scenario, where two causally independent parties A and C share each some resource with a central party B . (d) Arbitrary causal structures contain directed edges beyond the traditional network connections of latent-to-terminal edges and root-to-terminal edges. A method for analyzing correlations in general structures is given in Sec. IV.

the candidate Bayesian network is compatible if, and only if, all conditions in the hierarchy are satisfied [12].

When moving to quantum causal scenarios, the problem of causal compatibility presents several new features. In the classical case, the cardinality of the latent variables can be upper bounded [13] and, therefore, the problem is decidable. In the quantum case, however, a similar upper bound cannot exist because the problem of quantum causal compatibility is undecidable, as implied by recent results on quantum correlations [14, 15]. Yet, this does not preclude the existence of a method similar to inflation to tackle the question. Unfortunately, the inflation technique cannot be straightforwardly adapted to the quantum case because it relies on information broadcasting, a primitive that is not plausible with quantum information [16, 17]. Other causal analysis techniques which are fundamentally quantum have been proposed. Notably among these is the quantum entropy vector approach of Ref. [18], which is applicable to all causal structures but uses only those constraints on entropies imposed by the causal structure, or the scalar extension of Ref. [19], which imposes stronger constraints but cannot be applied to causal structures in which all observed nodes are causally connected, such as the triangle scenario of Fig. 1(b).

The main result of our work is the construction of **quantum inflation**, a systematic technique to study causal compatibility in any quantum Bayesian network. It can be seen as a quantum analogue of the classical inflation technique which avoids the latter's reliance on information broadcast. We first explain quantum inflation by example in Sec. II, then we provide a detailed construction for arbitrary two-layer DAGs in Sec. III. Sec. IV generalizes the technique to apply to *every* possible multi-layer causal structure involving unobserved quantum systems, utilizing the two-layer construction as its elementary constituent. Sec. V then considers a slight modification to quantum inflation

to obtain a new tool for assessing causal compatibility with classical models. In Sec. VI we apply quantum inflation to characterize correlations achievable in various tripartite quantum causal networks, including the derivation of quantum causal incompatibility witnesses. In Sec. VII we discuss the important further application of bounding the strength of causal effects (do-conditional estimation) in the presence of quantum common causes. Finally, we conclude in Sec. VIII.

II. QUANTUM INFLATION BY EXAMPLE

Consider the quantum causal network depicted in Fig. 2(a), whereby three random variables A , B , C (taking the values a, b, c) are generated by conducting bipartite measurements over the ends of three bipartite quantum states ρ_{AB} , ρ_{BC} , ρ_{AC} . We are handed the distribution $P_{\text{obs}}(a,b,c)$ of observed variables and asked if it is compatible with this model. How to proceed?

Suppose that there existed indeed bipartite states ρ_{AB} , ρ_{BC} , ρ_{AC} of systems $A''B'$, $B''C'$, $A'C''$, and commuting measurement operators E_a , F_b , G_c , acting on systems $A'A''$, $B'B''$, $C'C''$, respectively, which were able to reproduce the correlations $P_{\text{obs}}(a, b, c)$. Now imagine how the scenario would change if n independent copies ρ_{AB}^i , ρ_{BC}^i , ρ_{AC}^i , $i=1,\dots,n$ of each of the original states were distributed instead, as depicted in Fig. 2(b). Call ρ the overall quantum state before any measurement is carried out. For any $i, j = 1, \dots, n$ we can, in principle, implement measurement $\{E_a^i\}_a$ on the i^{th} copy of ρ_{AC} and the j^{th} copy of ρ_{AB} : we denote by $\{E_a^{i,j}\}_a$ the corresponding measurement operators. Similarly, call $\{F_b^{i,j}\}_b$, $\{G_c^{i,j}\}_c$ the measurement $\{F_b\}_b$ ($\{G_c\}_c$) over the states ρ_{AB}^i , ρ_{BC}^j (ρ_{BC}^i , ρ_{AC}^j).

The newly defined operators and their averages $\langle X \rangle_\rho := \text{tr}[\rho X]$ satisfy non-trivial relations. For

example, for $H=E,F,G$ and $i \neq k, j \neq l$ the operators $H_{-}^{i,j}$ and $H_{-}^{k,l}$ act on different Hilbert spaces, and hence $[H_{-}^{i,j}, H_{-}^{k,l}] = 0$. Similarly, expressions such as $\langle E_a^{1,1} E_{a'}^{1,2} F_b^{2,2} \rangle_{\rho}$ and $\langle E_a^{1,2} E_{a'}^{1,1} F_b^{1,2} \rangle_{\rho}$ can be shown identical, since one can arrive at the second one from the first one just by exchanging ρ_{AB}^1 with ρ_{AB}^2 . More generally, for any function $Q(\{E_a^{i,j}, F_b^{k,l}, G_c^{m,n}\})$ of the measurement operators and any three permutations π, π', π'' of the indices $1, \dots, n$, one should have

$$\begin{aligned} \langle Q(\{E_a^{i,j}, F_b^{k,l}, G_c^{m,n}\}) \rangle_{\rho} \\ = \langle Q(\{E_a^{\pi(i)}, F_b^{\pi'(j)}, G_c^{\pi''(l)}\}) \rangle_{\rho}. \end{aligned} \quad (1)$$

Finally, note that, if we conducted the measurements $\{E^{i,i}, F^{i,i}, G^{i,i}\}_{i=1}^n$ at the same time (something we can do, as they all commute with each other), then the measurement outcomes $a^1, \dots, a^n, b^1, \dots, b^n, c^1, \dots, c^n$ would be distributed according to

$$\left\langle \prod_{i=1}^n E_a^{i,i} F_b^{i,i} G_c^{i,i} \right\rangle_{\rho} = \prod_{i=1}^n P_{\text{obs}}(a^i, b^i, c^i). \quad (2)$$

If the original distribution $P_{\text{obs}}(a, b, c)$ is compatible with the network in Fig. 2(a), then there should exist a Hilbert space \mathcal{H} , a state $\rho : \mathcal{H} \rightarrow \mathcal{H}$ and operators $\{E_a^{i,j}\}_{i,j,a}$, $\{F_b^{k,l}\}_{k,l,b}$, $\{G_c^{m,n}\}_{m,n,c}$ satisfying the above relations. If such is the case, we say that $P_{\text{obs}}(a, b, c)$ admits an **n^{th} -order quantum inflation**. By increasing the index of n , we arrive at a hierarchy of conditions, each of which must be satisfied by any compatible distribution $P_{\text{obs}}(a, b, c)$.

At first glance, disproving the existence of a quantum inflation looks as difficult as the original feasibility problem. However, the former task can be tackled via non-commutative polynomial optimization (NPO) theory [20]. Originally developed to characterize quantum correlations in Bell scenarios [21, 22], the general goal of NPO theory is to optimize the expectation value of a polynomial over operators subject to a number of polynomial operator and statistical constraints. This is achieved by means of a hierarchy of semidefinite programming (SDP) tests [23], see also Appendix A. In our particular case, we are dealing with a feasibility problem. The polynomial operator constraints we wish to enforce on $E_a^{i,j}, F_b^{k,l}, G_c^{m,n}$ are that they define complete families of projectors, which commute when acting on different quantum systems. The statistical constraints are given by Eqs. (1-2). If for some n we were able to certify, via NPO theory, that $P_{\text{obs}}(a, b, c)$ does not admit an n^{th} -order quantum inflation, then we would have proven that $P_{\text{obs}}(a, b, c)$ does not admit a realization in the quantum network of Fig. 2(a). An application of this method for this precise scenario is given in Sec. VI A 1.

The method just described can be easily adapted to bound the statistics of any network in which the observed

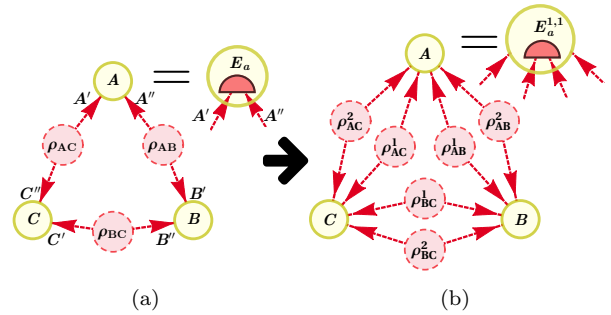


FIG. 2. Quantum inflation in the triangle scenario. (a) In the original scenario, by probing systems A' , A'' with the quantum measurement $\{E_a\}$, a value a for the random variable A is generated. The values b , c for the random variables B and C are produced similarly. (b) In quantum inflation, we distribute n (in the case shown, $n=2$) independent copies of the same states to the parties, which now use the original measurement operators on different pairs of copies of the states they receive. For instance, the measurement operators $\{E_a^{1,1}\}_a$ act on the states corresponding to copies ρ_{AB}^1 and ρ_{AC}^1 , and the measurements with other superindices are defined in an analogous way.

variables are defined by measurements on the quantum latent variables, such as the triangle scenario. To test the incompatibility of a distribution P_{obs} , we would consider a modified network with n copies of each of the latent variables, extend the original measurement operators to act on all possible copies of each system and work out how operator averages relate to P_{obs} and to each other. Finally, we would use NPO theory to disprove the existence of a state and operators satisfying the inferred constraints. In Sec. IV we further show how to extend the notion of quantum inflation to prove infeasibility in general quantum causal structures, where there might be causal connections among observed variables, as well as from observed to latent variables.

III. DETAILED DESCRIPTION

To illustrate the details of the construction, we first consider a subset of causal scenarios in which single measurements are applied to different quantum states. They correspond to two-layer DAGs in which arrows coming from a first layer, consisting in both observed and latent variables, go to a second layer of observed variables. Each of the variables in the second layer is regarded as an *outcome variable*, since it is the result of conducting a measurement on a quantum state. The tuple of values of all the classical observed parents of such a variable can be understood as the *measurement setting* used to produce this outcome; this is the case of, for instance, variables X , Y and Z in the tripartite-line scenario of Fig. 1(c).

The essential premise of quantum inflation is to ask what would happen if multiple copies of the original (un-

specified) quantum states were simultaneously available to each party. In this gedankenexperiment the parties use copies of their original measurement apparatus to perform n simultaneous measurements on the n copies of the original quantum states now available to them. There are different ways in which a party can align her measurements to act on the states now available, thus we must explicitly specify *upon which unique set* of Hilbert spaces a given measurement operator acts non-trivially. Let us therefore denote measurement operators by

$$\hat{O}_{i|m}^{s|k} \equiv \hat{O}(\text{Outcome variable}=k, \text{Spaces}=s, \text{Setting}=m, \text{Outcome}=i),$$

where the four indices specify

1. k , the index or name of the *outcome variable* in the original causal graph,
2. s , the Hilbert spaces the given operator acts on,
3. m , the measurement *setting* being used,
4. i , the *outcome* associated with the operator.

In the example of Fig. 2, we have

$$\begin{aligned} E_a^{i,j} &= E_a^{\{A'_i, A''_j\}} = \hat{O}_{a|\emptyset}^{\{A'_i, A''_j\}|A}, \\ F_b^{i,j} &= F_b^{\{B'_i, B''_j\}} = \hat{O}_{b|\emptyset}^{\{B'_i, B''_j\}|B}, \\ G_c^{i,j} &= G_c^{\{C'_i, C''_j\}} = \hat{O}_{c|\emptyset}^{\{C'_i, C''_j\}|C}. \end{aligned} \quad (3)$$

Now, using an $n=2$ quantum inflation as in Fig. 2(b), one would find that s for outcome variable $k=A$ may be sampled from precisely four possibilities, each value being a different *tuple*:

$$s \in \left\{ \{A'_1, A''_1\}, \{A'_1, A''_2\}, \{A'_2, A''_1\}, \{A'_2, A''_2\} \right\}.$$

where A'_i (A''_i) denotes the factor A of the Hilbert space where ρ_{AB}^i (ρ_{AC}^i) acts.

These operators will be regarded as the non-commuting variables of an NPO problem where the polynomial constraints are derived according to rules pertaining to the operators' projective nature and as well as a number of commutation rules. The statistical constraints are then imposed from symmetry under permutations of the state indices and enforcing consistency with the observed probabilities.

Projection rules

For fixed s, k, m , the non-commuting variables $\{\hat{O}_{i|m}^{s|k}\}_i$ must correspond to a complete set of measurement operators. Since we do not restrict the dimensionality of the Hilbert space where they act, we can take them to be a complete set of projectors. That is, they must obey the relations

$$\hat{O}_{i|m}^{s|k} = (\hat{O}_{i|m}^{s|k})^\dagger, \hat{O}_{i|m}^{s|k} \hat{O}_{i'|m}^{s|k} = \delta_{ii'} \hat{O}_{i|m}^{s|k}, \forall s, k, i, i', m \quad (3a)$$

$$\sum_i \hat{O}_{i|m}^{s|k} = 1, \text{ for all } s, k, m. \quad (3b)$$

These relations imply, in turn, that each of the noncommuting variables is a bounded operator. Hence, by [20], the hierarchy of SDP programs provided by NPO is complete, i.e., if the said distribution does not admit an n^{th} -order inflation, then one of the NPO SDP relaxations will detect its infeasibility.

Commutation rules

Operators acting on different Hilbert spaces must commute. More formally,

$$\left[\hat{O}_{i_1|m_1}^{s_1|k_1}, \hat{O}_{i_2|m_2}^{s_2|k_2} \right] = 0 \quad \text{if } s_1 \cap s_2 = \emptyset. \quad (4)$$

In Sec. V we consider modifying these commutation rules so as to construct an alternative SDP for constraining the correlations of *classical* causal structures.

Symmetry under permutations of the indices

The critical ingredient that relates the inflated network structure to the original network is that all averages of products of the noncommuting variables must be invariant under any permutation π of the source indices. Call ρ the overall quantum state of the inflated network (since we do not cap the Hilbert space dimension, we can assume that all state preparations in the original network are pure). Then we have that

$$\begin{aligned} & \left\langle \hat{O}_{i_1|m_1}^{s_1|k_1} \cdot \hat{O}_{i_2|m_2}^{s_2|k_2} \cdot \dots \cdot \hat{O}_{i_n|m_n}^{s_n|k_n} \right\rangle_\rho \\ &= \left\langle \hat{O}_{i_1|m_1}^{\pi(s_1)|k_1} \cdot \hat{O}_{i_2|m_2}^{\pi(s_2)|k_2} \cdot \dots \cdot \hat{O}_{i_n|m_n}^{\pi(s_n)|k_n} \right\rangle_\rho. \end{aligned} \quad (5)$$

An example of such statistical constraints imposed in the triangle scenario was given in Eq. (1). Another example, for an inflation level $n=3$, is the following:

$$\begin{aligned} & \left\langle E_0^{\{A'_1, A''_1\}} E_1^{\{A'_2, A''_2\}} F_0^{\{B'_1, B''_3\}} G_0^{\{C'_1, C''_1\}} \right\rangle_\rho \\ & \quad \text{apply } \rho_{AB}^1 \leftrightarrow \rho_{AB}^2 \end{aligned}$$

$$= \left\langle E_0^{\{A'_1, A''_2\}} E_1^{\{A'_2, A''_1\}} F_0^{\{B'_2, B''_3\}} G_0^{\{C'_1, C''_1\}} \right\rangle_\rho \quad (6a)$$

$$\begin{aligned} &= \left\langle E_0^{\{A'_1, A''_2\}} E_1^{\{A'_2, A''_3\}} F_0^{\{B'_2, B''_3\}} G_0^{\{C'_1, C''_1\}} \right\rangle_\rho \quad (6b) \\ & \quad \text{apply } \rho_{BC}^1 \leftrightarrow \rho_{BC}^3 \end{aligned}$$

$$= \left\langle E_0^{\{A'_1, A''_2\}} E_1^{\{A'_2, A''_3\}} F_0^{\{B'_2, B''_1\}} G_0^{\{C'_3, C''_1\}} \right\rangle_\rho, \quad (6c)$$

where, for readability, we identified $\hat{O}_{a|\emptyset}^{s|A}$ ($\hat{O}_{b|\emptyset}^{s|B}$) [$\hat{O}_{c|\emptyset}^{s|C}$] with E_a^s (F_b^s) [G_c^s] per Eq. (3).

Consistency with the observed probabilities

Finally, as described by Eq. (2) in Sec. II, certain expectation values pertaining to the inflated network can be related to products of the probabilities of P_{obs} . Let n be the order of the considered inflation. We first single out the j -th copy of each state, for $j=1,\dots,n$. For each random variable k , we write \vec{j}_k the set of Hilbert spaces on which k acts with the copy labels of all Hilbert spaces set to j (e.g.: $\vec{1}_A = \{A'_1, A''_1\}$, $\vec{2}_A = \{A'_2, A''_2\}$ in Fig. 2); we write $i_{j,k}$ for the measurement outcome of k and $m_{j,k}$ for its measurement setting, so we end up describing the operator $\hat{O}_{i_{j,k}|m_{j,k}}^{\vec{j}_k|k}$. For fixed j , the product of these operators over all random variables k has an expectation value that reproduces the observed probability distribution. Now, if we furthermore take the product of j over all n copies, the expectation value of the resulting operator reproduces n copies of the observed distribution. Formally, for any set of indices $\{i_{j,k}, m_{j,k}\}_{j,k}$, we have that

$$\left\langle \prod_{j=1}^n \prod_k \hat{O}_{i_{j,k}|m_{j,k}}^{\vec{j}_k|k} \right\rangle_{\rho} = \prod_{j=1}^n P_{\text{obs}} \left(\bigcap_k (i_{j,k}|m_{j,k}, k) \right), \quad (7)$$

where $(i|m, k)$ denotes the event of probing k with setting m and obtaining the result i .

The constraints (3), (4), (5) and (7) are satisfied by the overall state and operators involved in an n^{th} -order quantum inflation of a particular causal process with observed distribution P_{obs} . All have a form suitable to assess their physical realizability through NPO via a feasibility problem. Crucially, the left-hand side of (7), under the constraints (3)-(5), can be interpreted as a relaxation of the convex hull of n independent copies of a distribution P_{obs} compatible with the considered causal structure. Therefore, quantum inflation can be exploited not only for assessing whether an observed probability distribution can be generated in a particular quantum causal scenario, but also to optimize Bell-like polynomial expressions $B(P_{\text{obs}})$ over all quantum P_{obs} admitting a given causal explanation. For that, one renders the distribution P_{obs} also as an unknown. Now, the key idea is to express any Bell-like polynomial B as a linear combination of elements of the form $\left\langle \prod_j O_j \right\rangle$, via the correspondence (7). Minimizing or maximizing such a linear combination of expectation values can also be cast as a non-commutative polynomial optimization problem, that can be similarly tackled with NPO tools. In Sec. VI C we show an explicit example of how Eq. (7) is exploited in the optimization of polynomial Bell operators.

In fact, this idea can be generalized even further to carry optimizations over polynomials of arbitrary operator averages, i.e., not necessarily those averages related to products of observed probabilities. In this regard, the quantum inflation technique can also be applied for studying classical causal inference. We explain how to do so in Sec. V but, before that, we describe how

to extend the ideas above to arbitrary causal scenarios.

IV. ARBITRARY CAUSAL SCENARIOS

In the previous section we provided a systematic method to characterize the correlations achievable in a subset of quantum causal networks, namely two-layer DAGs where no node has both parents and children, and where every observable node has at most one observable parent. Let us denote such DAGs to have a **network form**. In this section we generalize all previous methodology to characterize correlations in arbitrary causal structures. Namely, we explain how an arbitrary causal structure can be reduced to network form cases, which we can already solve.

A. Visible nodes with parents and children: Maximal interruption

The first generalization we consider extends our techniques for network form DAGs to arbitrary so-called **latent exogenous** causal structures, where all unobserved nodes are root nodes but otherwise classical variables can have both parents and children.

We use the term **maximal interruption** to refer to our procedure for mapping the correlations of any latent-exogenous causal structure to the correlations of a unique network form structure. Graphically, interruption modifies a graph \mathcal{G} as follows: For every observed variable V which is neither a root node nor a terminal node, as well as for any V having multiple children, we introduce k new variables $\{V_i^{\#}\}_i$ where k denotes the number of edges outgoing from V . We then replace each edge formerly originating from V by an edge originating

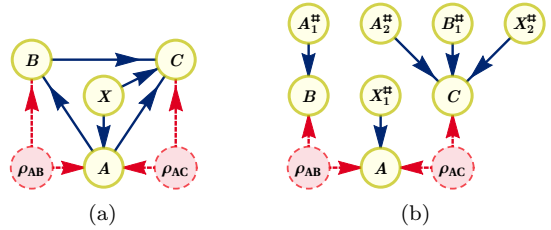


FIG. 3. An example causal structure (a) and its maximal interruption (b). Note that in (a) the observable nodes A and B both possess at least one parent node as well as at least one child node. Additionally, the observable nodes A and X have multiple child nodes. Constraints on distributions extended to the interrupted graph (such as those obtained via quantum inflation) are translated into constraints on the original distribution using the postselection relation $P_{3(a)}(A=a, B=b|X=x) = P_{3(b)}(A=a, B=b|X_1^{\#}=X_2^{\#}=x, A_1^{\#}=A_2^{\#}=a, B_1^{\#}=b)$.

from the corresponding $V_i^\#$. In the resulting (partially) *interrupted* graph \mathcal{G}' , V is a terminal node and every $V_i^\#$ is a root node. The correlations in \mathcal{G}' are related to those in the original graph \mathcal{G} by postselection, namely

$$P_{\mathcal{G}}(\dots, V=v) = P_{\mathcal{G}'}(\dots, V=v | V_1^\# = \dots = V_k^\# = v). \quad (8)$$

Proceeding in this fashion, any latent exogenous causal structure can be converted into a network form. A graphical example of interruption is shown in Fig. 3.

Distributions over the nodes of the interrupted graph \mathcal{G}' constitute *extensions* of distributions pertaining to the original graph. That is, observed statistics pertaining to \mathcal{G} only partially specify an extension to \mathcal{G}' . The following lemma specifies when a distribution over the nodes of the interrupted graph is a valid extension:

Fundamental Lemma of Interruption

$P'_{ABC|A^\#}$ is a valid extension of the original distribution P_{ABC} if and only if it is compatible with the interruption graph and recovers the original distribution under postselection. That is,

$$\begin{aligned} P'_{ABC|A^\#} &\in \text{ValidExtensions}_{\mathcal{G}'}[P_{ABC}] \\ \text{iff } P_{ABC}(abc) &= P'_{ABC|A^\#}(abc | a) \\ \text{and } P'_{ABC|A^\#} &\in \text{CompatibleDistributions}[\mathcal{G}']. \end{aligned} \quad (9)$$

Conceptually, interruption has extensive precedent in literature regarding classical causal analysis. It is a form of node-splitting [24], and hence is closely related to the Single-World Intervention Graphs (SWIGS) pioneered by Ref. [25], as well as the *e*-separation technique introduced in Ref. [26]. Interruption previously has been used to port Tsirelson inequalities constraining the set of quantum correlations compatible with the Bell scenario into constraints pertaining to the instrumental scenario [27] (see also the proof of Theorem 25 in Ref. [7]).

B. Latent nodes with parents

The remaining case that needs to be considered that of latent nonexogenous causal structures, where latent nodes can have parents. Evan's exogenization procedure [28] allows *classical* latent nonexogenous structures to be transformed into latent exogenous causal structures with the same predictive power. The procedure consists in replacing all arrows from a parent node to a latent node with arrows from the parent node to the children of the latent node. This operation is repeated for all parents of all latent nodes such that finally all latent variables become parentless.

When applied to quantum latent variables, however, exogenization results in a new quantum network that, in general, does not predict the same distributions of observed events as its predecessor. This is again related

to the impossibility of broadcasting quantum information [17]. The example in Fig. 4, evidencing this compatibility mismatch, is wholly due to Stefano Pironio.

To make the issue explicit, in Fig. 4(a) the variable S has the interpretation of a setting, which adjusts the state ρ_{BC} before it is sent to B and C . Thus, it is possible for $P(A,B|X,Y,S=0)$ to maximally violate a Bell inequality for A and B , and $P(A,C|X,Z,S=1)$ to maximally violate a Bell inequality for A and C . No quantum state prepared independently of S can do so, due to the monogamy of quantum correlations [29, 30]. Consequently, it is not possible to reproduce such correlations within the causal network of Fig. 4(b), product of applying Evan's exogenization to Fig. 4(a).

One way to deal with this predicament is to regard observable variables with unobserved children as random variables indicating the classical control of a quantum channel. In the same way, latent variables with latent children are treated as uncontrolled quantum channels (we defer to Appendix C the discussion that illustrates the need to account for this type of channels). Thus, in Fig. 4(a) we treat the root variable S as the classical control for a quantum channel acting on the BC subsystems. That is, one understands $\rho_{ABC|S=s} = \hat{U}_s \rho_{AS} \hat{U}_s^\dagger$, where, for all values of s , \hat{U}_s is a unitary operator that commutes with any operator acting solely on A 's subsystem. As such, the joint distribution of the values of the visible variables A, B, C conditioned on the root visible nodes can be understood as generated by

$$\begin{aligned} P(A=a, B=b, C=c | X=x, Y=y, Z=z, S=s) \\ = \left\langle \hat{U}_s^\dagger \hat{A}_x^a \hat{B}_y^b \hat{C}_z^c \hat{U}_s \right\rangle_{\rho_{AS}} = \left\langle \hat{A}_x^a \hat{U}_s^\dagger \hat{B}_y^b \hat{C}_z^c \hat{U}_s \right\rangle_{\rho_{AS}}. \end{aligned}$$

This interpretation can be made without loss of generality, since the subspace S of the complete Hilbert space AS can be understood as containing the subspaces corresponding to B and C .

As in the exogenous case, an n^{th} -order inflation of a causal structure with non-exogenous quantum

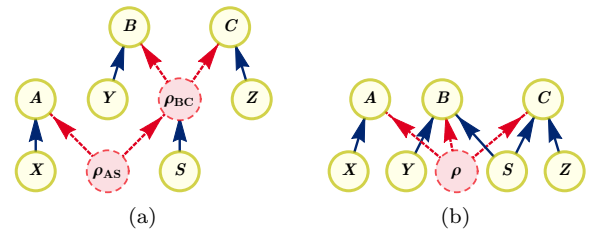


FIG. 4. In (a) there is a causal structure with ρ_{BC} being a nonexogenous unobserved quantum node. In (b) there is a different causal structure, corresponding to the classical latent reduction of the former. While these two graphs would be equivalent if the unobserved nodes were classical, they are demonstrably inequivalent when the unobserved nodes are quantum.

variables requires taking n copies of the unobserved root nodes. Each unitary operator \hat{U}_s in the original causal structure gives rise to operators of the form $\hat{O}_s^{\{S^j\}|U}$ in the inflated graph, where j denotes the copy of the Hilbert space where \hat{U}_s acts. The unitary or outcome operators associated to the descendants of any such “unitary node” (for instance, B and C , in Fig. 4) inherit the copy label j of the Hilbert space S^j .

With this last prescription, the symmetry relabelling rule, Eq. (5), still holds. However, the projection rules (3a-3b) only hold if the non-commuting variable k in question corresponds to an outcome variable in the original graph. If k corresponds to a unitary variable, then the operator $\hat{O}_m^{\mathbf{s}|k}$ must be subject to the constraints

$$\hat{O}_m^{\mathbf{s}|k}(\hat{O}_m^{\mathbf{s}|k})^\dagger = (\hat{O}_m^{\mathbf{s}|k})^\dagger \hat{O}_m^{\mathbf{s}|k} = \mathbb{1}. \quad (10)$$

The commutation rule (4) remains valid upon qualifying that the Hilbert spaces listed in $\mathbf{s}_1 \cup \mathbf{s}_2$ must be simultaneously co-existing in the original graph. For example, in Fig. 4(a), the operators corresponding to the Hilbert spaces associated to the outcome variables B and C co-exist after the transformation U_s is applied over system S . It follows that the corresponding measurement operators $O_{b|y}^{\mathbf{s}|B}, O_{c|z}^{\mathbf{s}'|C}$ commute. Finally, rule (7) expressing consistency with the observed probabilities must also be amended, to take into account that descendants of a unitary variable must be bracketed by the corresponding unitary and its adjoint.

Note that the aforementioned operator and statistical constraints are all polynomial, and thus they can all be enforced in the framework of NPO theory.

Interruption, classical exogenization, and the treatment for quantum exogenous variables hereby presented cover all possible nontrivial causal influences in arbitrary quantum causal structures. Quantum inflation is therefore a technique of full applicability to bound the quantum correlations achievable in any causal scenario.

V. SDP FOR CLASSICAL COMPATIBILITY

The quantum inflation technique can be easily adapted for solving the problem of causal compatibility with an arbitrary *classical* causal structure. It is known that any correlation achievable with only classical sources can be realized in terms of commuting measurements acting on a quantum state [31]. Therefore, in order to detect correlations incompatible with classical structures, one must generalize the commutation relations in the original quantum inflation method to the constraint that any pair of measurement operators commute. That is,

$$\hat{O}_{i_1|m_1}^{\mathbf{s}_1|k_1} \cdot \hat{O}_{i_2|m_2}^{\mathbf{s}_2|k_2} = \hat{O}_{i_2|m_2}^{\mathbf{s}_2|k_2} \cdot \hat{O}_{i_1|m_1}^{\mathbf{s}_1|k_1},$$

for all $\mathbf{s}_1, \mathbf{s}_2, k_1, k_2, m_1, m_2, i_1, i_2$. This defines a hierarchy of constraints that classical correlations compatible with a given causal structure must satisfy.

Contrary to the quantum case, the NPO hierarchy associated to a fixed inflation level is guaranteed to converge at a finite level. In fact, for NPO hierarchy levels higher than $N \cdot m \cdot (d-1)$ —where N is the number of parties, m is the number of settings per party and d is the number of outcomes per measurement—application of the commutation relations allows one to reduce any product of the operators involved into one of shorter length. For a fixed inflation level, the problem solved at the highest level of the NPO hierarchy is analogous to the linear program solved in classical inflation [11] at the same inflation level.

In contrast with the original classical inflation technique, the classical variant of the quantum inflation technique described in this article uses semidefinite programming, and exhibits far more efficient scaling with the inflation hierarchy than the original linear programming approach [12]. One must note that this gain in efficiency comes at the expense of introducing further relaxations in the problem. Nevertheless, this classical variant of quantum inflation is capable of recovering a variety of seminal results of classical causal compatibility, such as the incompatibility of the W and GHZ distributions with classical realizations in the triangle scenario. It also identifies the distribution described by Fritz [6], known to have a quantum realization in the triangle scenario, as incompatible with classical realizations. For all these results, the relaxed SDP formulation is far less memory-demanding than the raw linear programming formulation. Furthermore, the SDP approach is the only method that can be used when using inflation to assess causal compatibility in the presence of terminal nodes which can take continuous values.

In conclusion, not only can quantum inflation be leveraged to obtain results for networks with classical sources, but we argue that it is the most suitable technique to be used for addressing causal compatibility with classical realizations in large networks.

VI. RESULTS

In the following we demonstrate the power of quantum inflation by reproducing known results and solving open problems in different quantum causal scenarios.

A. Quantum Causal Compatibility

We begin by showing examples of specific probability distributions that we are able to identify as incompatible with various tripartite quantum causal networks. While quantum inflation applies to networks with observed variables of arbitrary cardinality, we hereafter consider scenarios involving exclusively two-output observed variables. We adopt the standard notations and label these outputs as $\{0,1\}$, unless otherwise specified.

1. The Triangle Scenario

We start with the simplest version of the triangle scenario consisting of three parties that are influenced in pairs by bipartite latent variables, as depicted in Fig. 1(b). The first example we study in this scenario is the so-called W distribution. This distribution is defined by the task of all parties outputting the outcome 0 except one, which should output 1. Explicitly, it is

$$P_W(a,b,c) := \begin{cases} \frac{1}{3} & a+b+c=1, \\ 0 & \text{otherwise.} \end{cases} \quad (11)$$

The W distribution was proven in Ref. [11] not to be realizable in the triangle scenario when the latent variables are classical. Additionally, it is easy to see that it is realizable with tripartite classical randomness. However, the question of whether the W distribution was realizable in the quantum triangle scenario remained open. It can be shown that P_W does not admit a second-order quantum inflation. Therefore, a quantum realization of the W distribution in the triangle scenario is impossible.

Quantum inflation is robust, and certifies that when mixing the W distribution with white noise, the resulting distribution $P_{W,v}(a,b,c) := vP_W(a,b,c) + (1-v)/8$ does not have a quantum realization in the triangle for all visibilities v higher than $3(2 - \sqrt{3}) \approx 0.8039$. This result is obtained by solving the NPO program associated to a second-order inflation and the set of monomials \mathcal{L}_2 (see Appendix B for the definition of this set), restricted to operators of length ≤ 3 .

2. The Triangle Scenario with Settings

As mentioned before, one can also consider more complicated networks that include additional observable variables to encode for choices of discrete measurement settings. Fig. 5 shows this type of network for the case of the triangle scenario. In this setup we study the Mermin-GHZ distribution, defined by $P_{\text{Mermin}}(a,b,c|x,y,z) :=$

$$\begin{cases} 1/8 & x+y+z=0 \pmod{2}, \\ (1+(-1)^{a+b+c})/8 & x+y+z=1, \\ (1-(-1)^{a+b+c})/8 & x+y+z=3. \end{cases} \quad (12)$$

Quantum inflation also allows one to prove that the Mermin-GHZ distribution is not compatible with a quantum realization in the triangle scenario with inputs, by showing that P_{Mermin} does not admit a second-order quantum inflation. Additionally, its noisy version $P_{\text{Mermin},v}$ can be proven not to have a quantum realization for any visibility v higher than $\sqrt{2}/3 \approx 0.8165$.

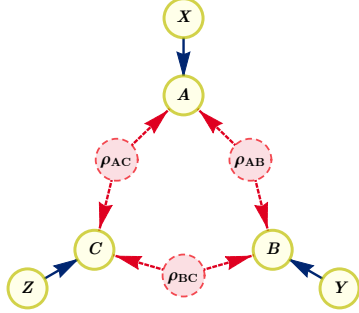


FIG. 5. The quantum triangle scenario with settings. Each of the visible variables A , B and C is now influenced not only by the latent variables, but from additional visible variables X , Y , Z that represent measurement choices.

3. The Tripartite-Line Scenario

Quantum inflation is organised as an infinite hierarchy of necessary conditions. There are however situations in which it recovers the quantum boundary at a finite step. An example of these situations is provided by the tripartite-line scenario of Fig. 1(c), which underlies phenomena such as entanglement swapping. The main characteristic of this structure is that there is no causal connection between the extreme variables A and C . As a consequence of this, all correlations realizable in the tripartite-line scenario satisfy the following factorization relation

$$\sum_b P_{\text{obs}}(a,b,c|x,y,z) = P_{\text{obs}}(a|x)P_{\text{obs}}(c|z). \quad (13)$$

This scenario has been thoroughly studied in the literature [32, 33]. In fact, it is known that the probability distribution

$$P_{\text{2PR}}(a,b,c|x,y,z) := [1 + (-1)^{a+b+c+xy+yz}]/8, \quad (14)$$

despite satisfying the constraint of Eq. (13), cannot be realized in the tripartite-line scenario in terms of classical or quantum latent variables. However, it is known that its mixture with white noise, $P_{\text{2PR},v} := vP_{\text{2PR}} + (1-v)/8$, can be realized if the visibility parameter v is sufficiently small [33]. $P_{\text{2PR},v}$ admits a realization in terms of quantum latent variables for any $0 \leq v \leq 1/2$, and in terms of classical latent variables for any $0 \leq v \leq 1/4$.

Quantum inflation correctly recovers that all $P_{\text{2PR},v}$ with visibility $v > 1/2$ are incompatible with the quantum tripartite-line scenario. It does so by certifying that for any $v > 1/2$, the corresponding $P_{\text{2PR},v}$ does not admit a second-order inflation, and this infeasibility is found already at the NPO hierarchy level corresponding to the set \mathcal{S}_2 (see Appendix B for a definition of this monomial set). Furthermore, we can also contrast against realizations in terms of classical latent variables by imposing

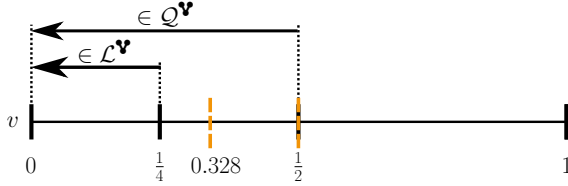


FIG. 6. Summary of results recoverable with quantum inflation in the tripartite-line scenario of Fig. 1(c) (orange, dashed lines). \mathcal{Q}^V and \mathcal{L}^V denote, respectively, the sets of quantum and classical correlations that can be generated in the tripartite-line scenario. Quantum inflation correctly recovers that all $P_{2\text{PR},v}$ with visibility $v > 1/2$ are incompatible with the quantum tripartite line scenario already at the NPO hierarchy finite level \mathcal{S}_2 when assessing compatibility with a second-order inflation. When imposing that all measurements commute, it witnesses that all $P_{2\text{PR},v}$ with visibility $v > 0.328$ cannot be realized in terms of classical hidden variables.

that all measurements in the problem commute. This classical version of quantum inflation, when analyzing compatibility with a third-order inflation, solving the NPO problem associated to the corresponding set of monomials \mathcal{L}_1 (its definition can be found in Appendix B), witnesses that all $P_{2\text{PR},v}$ with visibility $v > 0.328$ cannot be realized in terms of classical hidden variables. Lower values of this bound can in principle be achieved by considering higher inflation orders and larger monomial sets. The required computational capabilities for solving these problems, however, fall outside those provided by standard table-top computers.

B. Witnesses of Quantum Causal Incompatibility

A feature of semidefinite programming that has been widely employed in quantum information theory is the fact that the solution certificates of SDPs can be interpreted as Bell-like inequalities or witnesses that are capable of identifying correlations not attainable using the considered resources [22, 31]. The certificates obtained when using quantum inflation can have a similar interpretation as witnesses of quantum causal incompatibility. For instance, the certificate that provides the value of $v_{\max} = 6 - 3\sqrt{3} \approx 0.8039$ for the W distribution in the

quantum triangle scenario gives rise to the inequality

W's Certificate

$$\left(\begin{array}{l} -2P_{\text{inf}}(a^{\{A'_1, A''_1\}}) = 0 \\ +P_{\text{inf}}(a^{\{A'_1, A''_1\}}) = 0, a^{\{A'_2, A''_2\}} = 0 \\ -2P_{\text{inf}}(a^{\{A'_1, A''_1\}}) = 0, b^{\{B'_1, B''_1\}} = 0 \\ +4P_{\text{inf}}(a^{\{A'_1, A''_1\}}) = 0, b^{\{B'_2, B''_2\}} = 0 \\ -4P_{\text{inf}}(a^{\{A'_1, A''_1\}}) = 0, b^{\{B'_1, B''_1\}} = 0, \\ \quad a^{\{A'_2, A''_2\}} = 0, b^{\{B'_2, B''_2\}} = 0 \\ +2P_{\text{inf}}(a^{\{A'_1, A''_1\}}) = 0, a^{\{A'_2, A''_2\}} = 0, b^{\{B'_1, B''_1\}} = 0 \\ +2P_{\text{inf}}(a^{\{A'_1, A''_1\}}) = 0, b^{\{B'_1, B''_1\}} = 0, b^{\{B'_2, B''_2\}} = 0 \\ -2P_{\text{inf}}(a^{\{A'_1, A''_1\}}) = 0, b^{\{B'_1, B''_1\}} = 0, c^{\{C'_1, C''_2\}} = 0 \\ +[A \rightarrow B \rightarrow C \rightarrow A] + [A \rightarrow C \rightarrow B \rightarrow A] \end{array} \right) \leq 0, \quad (15)$$

where $+[A \rightarrow B \rightarrow C \rightarrow A]$ and $+[A \rightarrow C \rightarrow B \rightarrow A]$ mean repeating every term in the sum under the two cyclic permutations of subsystems, thereby implicitly tripling the coefficients of any cyclic-invariant terms. This certificate is defined in terms of a quantum distribution compatible with a second-order inflation of the triangle scenario. Now, by using the rules of Eq. (7) for consistency with the observed probabilities, this certificate can be transformed into a witness of tripartite distributions whose violation signals the distribution as being incompatible with a realization in the triangle scenario with quantum latent variables (note that we switch to the expectation-value picture¹):

W's Witness

$$\left(\begin{array}{l} \langle A \rangle + \langle A \rangle^2 - \langle A \rangle \langle AB \rangle - \langle A \rangle \langle AC \rangle \\ -2\langle BC \rangle + \langle B \rangle \langle C \rangle - \langle BC \rangle^2 - \langle A \rangle \langle B \rangle \langle C \rangle \\ +[A \rightarrow B \rightarrow C \rightarrow A] + [A \rightarrow C \rightarrow B \rightarrow A] \end{array} \right) \leq 3. \quad (16)$$

In fact, the W distribution of Eq. (11) attains a value of $3 + 8/9$ for this witness.

Remarkably, the witness obtained is polynomial in the elements of the probability distribution. This is in stark contrast with witnesses obtained through other techniques, which are either linear in the elements of the probability distribution or in the variables' entropies.

Exploiting SDP duality also enables us to obtain a polynomial witness for the infeasibility of the Mermin-

¹ This is obtained by performing the substitutions $p(i=0) = \frac{1}{2}(1 + \langle I \rangle)$, $p(i=0, j=0) = \frac{1}{4}(1 + \langle I \rangle + \langle J \rangle + \langle IJ \rangle)$.

GHZ distribution box discussed in Sec. VI A 2, namely

Mermin Box Polynomial Witness

$$\begin{cases} +1 & \left(\begin{array}{l} \langle A_0 B_0 C_0 \rangle^2 \\ + \langle A_0 B_1 C_1 \rangle^2 \\ + \langle A_1 B_0 C_1 \rangle^2 \\ + \langle A_1 B_1 C_0 \rangle^2 \end{array} \right) \\ +2 & \left(\begin{array}{l} \langle A_0 B_1 C_1 \rangle \langle A_1 B_0 C_1 \rangle \\ + \langle A_0 B_1 C_1 \rangle \langle A_1 B_1 C_0 \rangle \\ + \langle A_1 B_0 C_1 \rangle \langle A_1 B_1 C_0 \rangle \end{array} \right) \\ +3 & \left(\begin{array}{l} \langle A_1 B_1 C_1 \rangle^2 \\ + \langle A_0 B_0 C_1 \rangle^2 \\ + \langle A_0 B_1 C_0 \rangle^2 \\ + \langle A_1 B_0 C_0 \rangle^2 \end{array} \right) \\ +6 & \left(\begin{array}{l} \langle A_0 B_0 C_1 \rangle \langle A_0 B_1 C_0 \rangle \\ + \langle A_0 B_0 C_1 \rangle \langle A_1 B_0 C_0 \rangle \\ + \langle A_0 B_1 C_0 \rangle \langle A_1 B_0 C_0 \rangle \end{array} \right) \\ -2 & \langle A_0 B_0 C_0 \rangle \left(\begin{array}{l} \langle A_0 B_1 C_1 \rangle \\ + \langle A_1 B_0 C_1 \rangle \\ + \langle A_1 B_1 C_0 \rangle \end{array} \right) \\ -6 & \langle A_1 B_1 C_1 \rangle \left(\begin{array}{l} \langle A_0 B_0 C_1 \rangle \\ + \langle A_0 B_1 C_0 \rangle \\ + \langle A_1 B_0 C_0 \rangle \end{array} \right) \end{cases} \leq 32. \quad (17)$$

In particular, this witness recognizes 15 out of the 45 nonlocal extremal points of the tripartite nonsignaling scenario [34] as not realizable in the quantum triangle

scenario.²

C. Optimization in Quantum Causal Scenarios

As explained in Sec. III, the constraints (3), (4), (5) and (7) characterize relaxations of the set of quantum correlations compatible with a given causal structure. This characterization can be employed to easily bound optimal values of polynomials of the measurement operators in the problem via NPO theory [20].

1. Optimization of linear functionals

First, we give some examples of applications of this procedure by finding upper bounds to the maximum value that certain Bell-like operators can achieve in the quantum triangle scenario. The results herein have been obtained by considering second-order inflations, solving the associated NPO problems with the set of monomials $\mathcal{S}_2 \cup \mathcal{L}_1$. Including the identity operator, we find that each party has 9 possible operators at this SDP level, such that the resulting moment matrix involved in the calculations has size 873×873 .

Mermin's Inequality [35]

$$\langle A_1 B_0 C_0 \rangle + \langle A_0 B_1 C_0 \rangle + \langle A_0 B_0 C_1 \rangle - \langle A_1 B_1 C_1 \rangle \leq \begin{cases} 2 & \mathcal{L}^\Delta, \mathcal{L}^\Delta \\ 3.085^* & \mathcal{Q}^\Delta \\ 4 & \mathcal{Q}^\Delta, \mathcal{NS}^\Delta, \mathcal{NS}^\Delta \end{cases} \quad (18)$$

Svetlichny's Inequality [36]

$$\begin{aligned} \langle A_1 B_0 C_0 \rangle + \langle A_0 B_1 C_0 \rangle + \langle A_0 B_0 C_1 \rangle - \langle A_1 B_1 C_1 \rangle \\ - \langle A_0 B_1 C_1 \rangle - \langle A_1 B_0 C_1 \rangle - \langle A_1 B_1 C_0 \rangle + \langle A_0 B_0 C_0 \rangle \leq \begin{cases} 4 & \mathcal{L}^\Delta, \mathcal{L}^\Delta \\ 4.405^* & \mathcal{Q}^\Delta \\ 4\sqrt{2} & \mathcal{Q}^\Delta \\ 8 & \mathcal{NS}^\Delta, \mathcal{NS}^\Delta \end{cases} \end{aligned} \quad (19)$$

The triangle Δ denotes the causal triangle scenario, while Δ refers to the standard tripartite Bell scenario. Clearly, for any set $\mathcal{X} = \{\mathcal{L}, \mathcal{Q}, \mathcal{NS}\}$, the bound obtained in \mathcal{X}^Δ is smaller or equal than the one obtained in \mathcal{X}^Δ . The asterisk means that the values given are upper bounds; that is, quantum inflation shows that Mermin's and Svetlichny's inequalities cannot exceed 3.085 or 4.405, respectively, in the quantum triangle scenario, but, at the moment, it is unknown whether those values are attainable.

It is known that both the algebraic maximum of 4 for Mermin's inequality and the algebraic maximum of 8 for Svetlichny's inequality can be achieved in the triangle structure, if one considers that the latent nodes distribute nonsignaling resources (see, for instance, [37, Sec. III-C]). This means that no difference between the triangle and the Bell scenarios can be identified with these two inequalities when the latent variables represent nonsignaling resources, i.e., $\max_{\mathcal{NS}^\Delta} = \max_{\mathcal{NS}^\Delta}$ for these two inequalities. Consequently, our finding here that $\max_{\mathcal{Q}^\Delta} < \max_{\mathcal{Q}^\Delta}$ for these two inequalities cannot be recovered by means of the GPT-valid (non-fanout) variant of the inflation method considered in Ref. [11, Sec. V-D].

² In the ordering of Ref. [34], the incompatible boxes are numbers 2, 13, 21, 22, 27, 29, 30, 31, 34, 36, 39, 41, 43, 44 and 46.

In a similar manner, the maximum values attainable by any linear function in the classical triangle and Bell scenarios also coincide, because even though $\mathcal{L}^\Delta \subsetneq \mathcal{L}^\Delta$, the *extremal* correlations in \mathcal{L}^Δ are also members of the set \mathcal{L}^Δ , as the local deterministic strategies are product correlations.

Remarkably, we see a divergence in linear-function optimization over Δ and Δ when considering quantum latent variables. In the quantum triangle scenario it is not possible to saturate such inequalities up to the bounds attainable in the quantum Bell scenario. This has the implication that having access to tripartite quantum resources allows for improved performance in information tasks relative to having access to arbitrary bipartite quantum states and unlimited shared randomness [38].

Recall that while polynomial functions may differ over the triangle scenarios with and without shared randomness, *linear*-function optimization is independent of the presence or absence of shared randomness. That is, even though $\mathcal{Q}^\Delta \subsetneq \mathcal{Q}^{\Delta+\text{SR}} \subsetneq \mathcal{Q}^\Delta$, it is the case that $\mathcal{Q}^{\Delta+\text{SR}}$ is the convex hull of \mathcal{Q}^Δ . This demonstrates that the Mermin-GHZ box of Eq. (12) is not achievable in $\mathcal{Q}^{\Delta+\text{SR}}$, a result relevant to Ref. [39].

The values 3.085 and 4.405 given for \mathcal{Q}^Δ in Eqs. (18) and (19) represent upper bounds to the real maximum values achievable. We can readily establish, respectively, lower bounds of $2\sqrt{2}$ and 4 by considering explicit bipartite quantum correlations for Alice and Bob and taking Charlie to always answer +1. It is an open question whether, when increasing the inflation and NPO hierarchies, one will find that the values for \mathcal{Q}^Δ will collapse to those lower bounds.

2. Optimization of non-linear functionals

Our tools can also be used to optimize over a non-linear witness f . The essential idea can be seen already in Sec. VI B, where Eq. (7) related linear functions in an inflation to polynomials in the corresponding original scenario. Note that, for this to be possible, in general one must consider at least an order- q inflation when optimizing a polynomial of degree q .

Consider, for instance, minimizing the 2-norm between a distribution $P_{\text{obs}}(a,b,c)$ achievable in the quantum triangle scenario and that of the W distribution, that is:

$$\begin{aligned} f(P_{\text{obs}}) &\equiv \sum_{a,b,c=0,1} |P_{\text{obs}}(a,b,c) - P_{\text{W}}(a,b,c)|^2 \\ &= \sum_{a,b,c=0,1} [P_{\text{obs}}(a,b,c)^2 + P_{\text{W}}(a,b,c)^2 \\ &\quad - 2P_{\text{obs}}(a,b,c)P_{\text{W}}(a,b,c)], \end{aligned} \quad (20)$$

where one can readily verify that $\sum_{a,b,c} P_{\text{W}}(a,b,c)^2 = 1/3$.

One can estimate the minimum value of this function using 2nd-order inflation or higher, via Eq. (7). In particular, have have

$$P_{\text{obs}}(a,b,c)^2 = \left\langle E_a^{1,1} E_a^{2,2} F_b^{1,1} F_b^{2,2} G_c^{1,1} G_c^{2,2} \right\rangle,$$

$$\text{and } P_{\text{obs}}(a,b,c)P_{\text{W}}(a,b,c) = P_{\text{W}}(a,b,c) \left\langle E_a^{1,1} F_b^{1,1} G_c^{1,1} \right\rangle.$$

While obtaining nontrivial bounds on $f(P_{\text{obs}})$ is in principle possible, in practice it appears to require levels of the NPO hierarchy too computationally expensive.

VII. BOUNDING CAUSAL EFFECTS UNDER QUANTUM CONFOUNDING

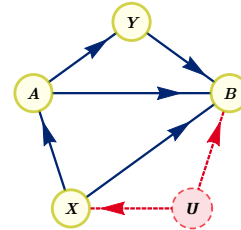


FIG. 7. A graph admitting multiple causal explanations for correlation between A and B .

Reichenbach's Common Causal Principle states that all nonspurious statistical correlations must admit some causal explanation, and this can be generalized to include quantum causal explanations as well [8, 10, 40, 41]. Often, however, one may wish to distinguish between various causal possibilities for establishing statistical correlation. Moreover, even knowledge of the true causal structure is still inferior to a complete understanding of functional relationships between observable variables. Consider the multiple possible causal explanations for correlation between variables A and B in Fig. 7, we have:

- The *direct effect* of A on B , associated with the edge $A \rightarrow B$.
- The *indirect effect* of A on B , associated with the *direct path* $A \rightarrow Y \rightarrow B$.
- The *common dependence* of A and B on X , associated with the *forking path* $A \leftarrow X \rightarrow B$.
- The *common dependence* of A and B on U , associated with the *forking path* $A \leftarrow X \leftarrow U \rightarrow B$.

Of course, in reality the true causal explanation of a correlation typically involves *all* these routes. The subfield of causal inference known as **mediation analysis** provides definitions of effect strength parameters for quantifying the relative significance of different causal pathways [42–45]. Such measures are generally intended to distinguish between:

- The *total causal effect* of A on B , associated with *all* paths originating at A and terminating at B , and

- Everything else, namely the *total common cause dependence* shared between A and B , associated with *all* their common ancestors.

Latent **confounding** is the possibility of partially explaining a pair of variables' observed correlation in terms of the functional dependence on their unobserved common causes. Estimating (or identifying) the strength of causal effects in the presence of latent confounding is the subject of extensive research [43–50]; our contribution in this section is to unlock the possibility of effect estimation in the presence of quantum latent confounding by using quantum inflation.

The most well-studied measure of effect strength is the **average causal effect (ACE)** which quantifies of how much one variable B functionally depends on another A . It is defined as the variation in the expectation value of B under intervention of different values for A . Formally,

$$\text{ACE}[a_1, a_2, B] := \langle B \text{ do } a_1^{\#} \rightarrow B \rangle - \langle B \text{ do } a_2^{\#} \rightarrow B \rangle \quad (21)$$

with $\text{ACE}[A, B] := \max_{a_1, a_2} \text{ACE}[a_1, a_2, B]$.

Note that the distribution of B under *intervention* on A has a meaning distinct from conditioning on A . When A and B share some common causal ancestry, typically

$$P(B|\{A=a\}) \neq P(B \text{ do } \{A^{\#}=a\} \rightarrow B), \quad (22)$$

where the notation $\{A^{\#}=a\} \rightarrow B$ indicates that the value of A *as seen by* B has been artificially set to a , independent of the actual value of A that may have been observed. For a review of do-conditionals and distinction between passive (observational) and active (interventional) conditioning, we refer the reader to Refs. [44, 46–48]. The fundamental lemmas of mediation analysis constrain the possible values of interventional do-conditionals from knowledge of both the underlying causal structure and the distribution under passive observation. Every do-conditional can be expressed in terms of extending the original distribution to a particular interruption of the original graph.

When estimating the do-conditional $\{A^{\#}=a^{\#}\} \rightarrow B$, the interrupted graph \mathcal{G}' is formed by replacing the $A \rightarrow B$ edge-set in \mathcal{G} with $A^{\#} \rightarrow B$, such that \mathcal{G}' contains the *additional* variables $A^{\#}$. Whenever P_{ABC} is defined over the observed variables $\{A, B, C\}$, then the extended distribution $P'_{ABC|A^{\#}}$ further pertains to the variables $A^{\#}$ as well. Note that this is precisely the fundamental lemma of interruption (9) merely being applied to the interrupted graph representing the *particular* do-conditional in lieu of the maximal interruption graph defined in Sec. IV A.

Thus, in general, mediation analysis relies on the following lemmas:

Fundamental Lemmas of Mediation Analysis:

1. $P'_{ABC|A^{\#}}$ is a valid extension of the original distribution P_{ABC} if and only if it is compatible with the interrupted graph and recovers the original distribution under postselection. That is,

$$\begin{aligned} P'_{ABC|A^{\#}} &\in \text{ValidExtensions}_{\mathcal{G}'}[P_{ABC}] \\ \text{iff } P_{ABC}(abc) &= P'_{ABC|A^{\#}}(abc|a) \quad (9) \\ \text{and } P'_{ABC|A^{\#}} &\in \text{CompatibleDistributions}[\mathcal{G}']. \end{aligned}$$

2. Every do-conditional can be expressed as some extended distribution or suitable marginal thereof. Accordingly, the potential range of a do-conditional is defined by variation over all valid extensions of the original distributions. Taking $M[\cdot]$ to indicate some arbitrary marginalization over some subset of the observable variables in \mathcal{G} , we have

$$\begin{aligned} M[P_{ABC} \text{ do } A^{\#} \rightarrow B] &\in \text{PotentialEffects}_{\mathcal{G}'}[P_{ABC}] \\ \text{iff } \exists: P'_{ABC|A^{\#}} &\in \text{ValidExtensions}_{\mathcal{G}'}[P_{ABC}] \quad (23) \\ \text{such that } M[P_{ABC} \text{ do } A^{\#} \rightarrow B] &= M[P'_{ABC|A^{\#}}]. \end{aligned}$$

Note that the first is the Fundamental Lemma of Interruption of Eq. (9), reproduced here for clarity.

For the purposes of this work, we emphasize that mediation analysis explicitly maps the problem of bounding causal effects to the problem of causal compatibility relative to a interrupted graph. In particular, mediation analysis implies that the quantum inflation technique can provide upper and lower bounds for the *quantum ACE*, i.e., can constrain causal effects in the presence of quantum confounding. For instance, quantum ACE can be lower (upper) bounded by minimizing (maximizing) $\text{ACE}[a_1, a_2, B]$ over extended distributions which are quantum-compatible with the graph interruption corresponding to replacing the edge $A \rightarrow B$ with the edge $A^{\#} \rightarrow B$.

An important result in mediation analysis is that some do-conditionals are constrained to a single point value (called *identifiable*) regardless of the particular observed statistics. The criteria for determining identifiable do-conditional (and efficient algorithms for computing their values) is the subject of Refs. [44–48]. Non-identifiable do-conditionals can typically only be constrained to lie within certain numerical spans [43, 49, 50].³ Visual examples of some identifiable and non-identifiable do-conditionals are provided in Fig. 8.

We note that the criteria for determining identifiability are valid independent of the (non)classicality

³ Fine-tuned instances of the observable distribution can constrain a non-identifiable do-conditional to the point where it can only take some extremal fixed value.

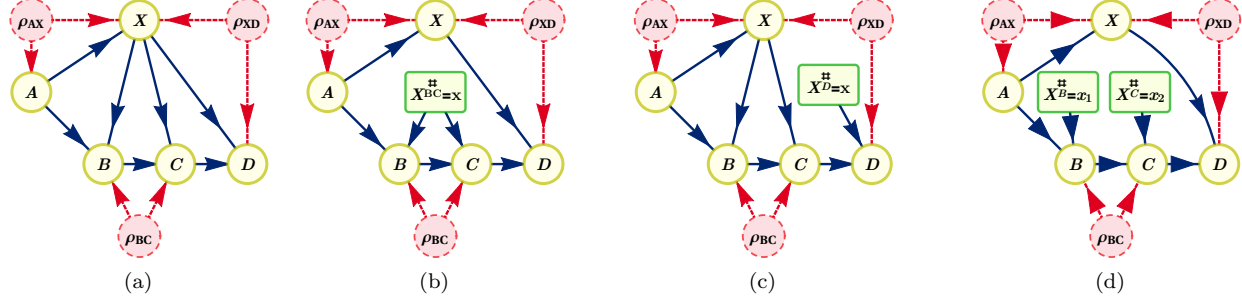


FIG. 8. A survey of hypothetical interventions on edges emanating from the node X in a pedagogically motivated example causal structure.

(a) The example causal structure without any interventions.
 (b) The do-conditional $P(ABCDX \text{ do } \{X^\# = x^\#\} \rightarrow \{BC\})$ where both edges $X \rightarrow B$ and $X \rightarrow C$ are intervened upon with the same value of X being sent down both intervened edges. This is an identifiable do-conditional, and has a unique value computable from observational statistics alone, namely $P(ABCDX=x \text{ do } \{X^\# = x^\#\} \rightarrow \{BC\}) = P(ABCDX=x)P(BC|A, X=x^\#)/P(BC|A, X=x)$.
 (c) The do-conditional $P(ABCDX \text{ do } \{X^\# = x^\#\} \rightarrow D)$ where the edge $X \rightarrow D$ is intervened upon. This is a non-identifiable do-conditional (as X and D share a latent parent), and hence is interesting to estimate using quantum inflation.
 (d) The do-conditional $P(ABCDX \text{ do } \{X^\# = x_1^\#\} \rightarrow B, \{X^\# = x_2^\#\} \rightarrow C)$ where the pair of edges $X \rightarrow B$ and $X \rightarrow C$ are intervened upon with a different value of X being sent down the two intervened edges. This is a non-identifiable do-conditional (as B and C share a latent parent), and hence is interesting to estimate using quantum inflation.

of the latent variables. Consequently, quantum and classical mediation analysis can differ only in terms of the inequalities they imply for ranges of non-identifiable do-conditionals. Ref. [51] highlighted that this difference indeed exists by constructing a quantum causal model for the instrumental scenario where the quantum average causal effect is zero even though the resulting observational distribution would necessarily imply a strictly positive classical ACE.

To illustrate the utility of quantum inflation for mediation analysis, consider the quantum triangle scenario supplemented by a directed edge $A \rightarrow B$, illustrated in Fig. 9(a). The GHZ distribution

$$P_{\text{GHZ}}(a, b, c) := \begin{cases} \frac{1}{2} & a=b=c \\ 0 & \text{otherwise} \end{cases} \quad (24)$$

is compatible with this graph. To achieve this correlation, however, we anticipate that B must *functionally* depend on A . However, $P_B \text{ do } A^\# \rightarrow B$ is not identifiable, as A and B share an unobserved common parent. We employed the quantum inflation technique to verify that the $\text{ACE}[A, B] = 1$ for the GHZ distribution without assuming classicality, thus teaching us that the quantum ACE is *not* less than the classical ACE in this example. This means that, when reproducing the GHZ distribution in the quantum triangle scenario with signalling per Fig. 9(a), the functional dependence of B on the signal from A cannot be reduced relative to the strong dependence of B on A required to reproduce the GHZ distribution in the classical triangle scenario with signalling. This is in stark contrast to the example

in Ref. [51] where an instrumental scenario correlation requires reduced functional dependence between the observable variables when the latent node is quantum versus when it is classical.

VIII. CONCLUSIONS

We introduced the quantum inflation technique, a systematic method to discern whether an observable distribution is compatible with a causal explanation involving quantum degrees of freedom. The technique is of general applicability, in that it can be employed to analyze correlations achievable by any quantum causal structure with, potentially, visible-to-visible,

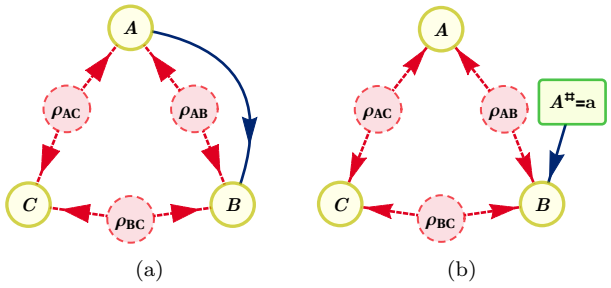


FIG. 9. (a) The triangle scenario supplemented with a directed edge from $A \rightarrow B$. (b) The relevant interrupted graph used to both define and compute the ACE of A on B .

latent-to-visible, visible-to-latent or latent-to-latent connections. Furthermore, we discussed how a slight modification allows also to study causal realizations in terms of classical latent variables.

We used quantum inflation to study correlations achievable in different quantum causal structures. First, we proved that the W and Mermin-GHZ distributions cannot be generated in the triangle scenario with quantum latent variables and bounded their noise resistance, and showed how quantum inflation is capable of recovering known results in the entanglement swapping scenario. Moreover, exploiting the dual formulation of semidefinite programs, we derived polynomial quantum causal witnesses for the triangle scenario with and without inputs. Second, we showed how quantum inflation can be employed as a tool for constrained polynomial optimization. We illustrated this by bounding the maximum values achievable by Mermin's and Svetlichny's inequalities in the quantum triangle scenario, and found important gaps relative to the values achievable when one has access to arbitrary three-way entanglement. Finally, we illustrated the applicability of quantum inflation for mediation analysis in the presence of quantum common causes.

The implementation of quantum inflation comprises two different hierarchies: the one of inflations, and for each inflation, the NPO hierarchy used to determine whether a distribution admits such an inflation. While asymptotic convergence has been proven for the latter, that of the former is an open question. Nevertheless, we have identified situations in which tight results can be obtained at finite steps of the hierarchies. Moreover, recent results [52] show that a convergent NPO hierarchy can be defined for the analysis of quantum correlations in sequential Bell scenarios. Given that many nonexogenous causal structures with unobserved children that have only visible parents can be mapped to networks linking such sequential

scenarios (though not all, as shown in Appendix C), Ref. [52]'s proof becomes an interesting starting point.

Quantum inflation can find an application in many fields. Clear first applications are generalizations of entanglement theory and quantum information protocols to networks [38, 39]. From a more general perspective, and due to the central role that causality has in science, we expect quantum inflation to become a fundamental tool for analyzing causality in any situation where a quantum behavior is presumed.

ACKNOWLEDGMENTS

We acknowledge useful discussions with Stefano Pironio, Rob Spekkens, David Schmid, and T.C. Fraser. This work is supported by Fundació Obra Social “la Caixa” (LCF/BQ/ES15/10360001), the ERC through the AdG CERQUTE and the CoG QITBOX, the European Union’s Horizon 2020 research and innovation programme - grant agreement No 648913, the AXA Chair in Quantum Information Science, the Spanish MINECO (Severo Ochoa SEV-2015-0522), Fundació Cellex and Mir-Puig, Generalitat de Catalunya (SGR 1381 and CERCA Programme) and the Austrian Science fund (FWF) stand-alone project P 30947. This research was supported by Perimeter Institute for Theoretical Physics. Research at Perimeter Institute is supported in part by the Government of Canada through the Department of Innovation, Science and Economic Development Canada and by the Province of Ontario through the Ministry of Colleges and Universities. This publication was made possible through the support of a grant from the John Templeton Foundation. The opinions expressed in this publication are those of the authors and do not necessarily reflect the views of the John Templeton Foundation.

[1] J. Pearl, *Causality: Models, Reasoning, and Inference* (Cambridge University Press, 2009).

[2] S. Morgan and C. Winship, *Counterfactuals and Causal Inference: Methods and Principles for Social Research* (Cambridge University Press, 2007).

[3] I. Shpitser and J. Pearl, “Complete identification methods for the causal hierarchy,” *J. Mach. Learn. Res.* **9**, 1941 (2008).

[4] J. S. Bell, “On the problem of hidden variables in quantum mechanics,” *Rev. Mod. Phys.* **38**, 447 (1966).

[5] N. Brunner, D. Cavalcanti, S. Pironio, V. Scarani, and S. Wehner, “Bell nonlocality,” *Rev. Mod. Phys.* **86**, 419 (2014).

[6] T. Fritz, “Beyond Bell’s theorem: correlation scenarios,” *New J. Phys.* **14**, 103001 (2012).

[7] J. Henson, R. Lal, and M. F. Pusey, “Theory-independent limits on correlations from generalized Bayesian networks,” *New J. Phys.* **16**, 113043 (2014).

[8] C. J. Wood and R. W. Spekkens, “The lesson of causal discovery algorithms for quantum correlations: causal explanations of Bell-inequality violations require fine-tuning,” *New J. Phys.* **17**, 033002 (2015).

[9] R. Chaves, R. Kueng, J. Bohr Brask, and D. Gross, “Unifying framework for relaxations of the causal assumptions in bell’s theorem,” *Phys. Rev. Lett.* **114**, 140403 (2015).

[10] E. Wolfe, D. Schmid, A. Belén Sainz, R. Kunjwal, and R. W. Spekkens, “Quantifying Bell: The resource theory of nonclassicality of common-cause boxes,” *arXiv:1903.06311* (2019).

[11] E. Wolfe, R. W. Spekkens, and T. Fritz, “The Inflation Technique for causal inference with latent variables,” *J. Causal Inference* **7** (2019).

[12] M. Navascués and E. Wolfe, “The Inflation Technique completely solves the causal compatibility problem,” [arXiv:1707.06476](https://arxiv.org/abs/1707.06476) (2017).

[13] D. Rosset, N. Gisin, and E. Wolfe, “Universal bound on the cardinality of local hidden variables in networks,” *Quant. Info. & Comp.* **18**, 910 (2018).

[14] W. Slofstra, “The set of quantum correlations is not closed,” *For. Math., Pi* **7**, e1 (2019).

[15] Z. Ji, A. Natarajan, T. Vidick, J. Wright, and H. Yuen, “MIP*=RE,” [arXiv:2001.04383](https://arxiv.org/abs/2001.04383) (2020).

[16] H. Barnum, C. M. Caves, C. A. Fuchs, R. Jozsa, and B. Schumacher, “Noncommuting mixed states cannot be broadcast,” *Phys. Rev. Lett.* **76**, 2818 (1996).

[17] H. Barnum, J. Barrett, M. Leifer, and A. Wilce, “Cloning and broadcasting in generic probabilistic theories,” [quant-ph/0611295](https://arxiv.org/abs/0611295) (2006).

[18] R. Chaves, C. Majenz, and D. Gross, “Information-theoretic implications of quantum causal structures,” *Nat. Commun.* **6** (2015).

[19] A. Pozas-Kerstjens, R. Rabelo, L. Rudnicki, R. Chaves, D. Cavalcanti, M. Navascués, and A. Acín, “Bounding the sets of classical and quantum correlations in networks,” *Phys. Rev. Lett.* **123**, 140503 (2019).

[20] S. Pironio, M. Navascués, and A. Acín, “Convergent relaxations of polynomial optimization problems with non-commuting variables,” *SIAM J. Optim.* **20**, 2157 (2010).

[21] M. Navascués, S. Pironio, and A. Acín, “Bounding the set of quantum correlations,” *Phys. Rev. Lett.* **98**, 010401 (2007).

[22] M. Navascués, S. Pironio, and A. Acín, “A convergent hierarchy of semidefinite programs characterizing the set of quantum correlations,” *New J. Phys.* **10**, 073013 (2008).

[23] L. Vandenberghe and S. Boyd, “Semidefinite programming,” *SIAM Rev.* **38**, 49 (1996).

[24] J. Barrett, R. Lorenz, and O. Oreshkov, “Quantum causal models,” [arXiv:1906.10726](https://arxiv.org/abs/1906.10726) (2019).

[25] T. S. Richardson and J. M. Robins, *Single World Intervention Graphs (SWIGs) : A Unification of the Counterfactual and Graphical Approaches to Causality* (Now Publishers Inc, 2013) Working Paper #128, Center for Stat. & Soc. Sci., U. Washington.

[26] R. J. Evans, “Graphical methods for inequality constraints in marginalized DAGs,” in *IEEE International Workshop on Machine Learning for Signal Processing* (2012).

[27] T. Van Himbeeck, J. Bohr Brask, S. Pironio, R. Ramanathan, A. B. Sainz, and E. Wolfe, “Quantum violations in the Instrumental scenario and their relations to the Bell scenario,” *Quantum* **3**, 186 (2019).

[28] R. J. Evans, “Margins of discrete Bayesian networks,” *Annals Stat.* **46**, 2623 (2018).

[29] B. Toner, “Monogamy of non-local quantum correlations,” *Proc. Roy. Soc. A* **465**, 59 (2009).

[30] M. P. Seevinck, “Monogamy of correlations versus monogamy of entanglement,” *Quant. Info. Proc.* **9**, 273 (2010).

[31] F. Baccari, D. Cavalcanti, P. Wittek, and A. Acín, “Efficient device-independent entanglement detection for multipartite systems,” *Phys. Rev. X* **7**, 021042 (2017).

[32] C. Branciard, N. Gisin, and S. Pironio, “Characterizing the nonlocal correlations created via entanglement swapping,” *Phys. Rev. Lett.* **104**, 170401 (2010).

[33] C. Branciard, D. Rosset, N. Gisin, and S. Pironio, “Bilocal versus nonbilocal correlations in entanglement-swapping experiments,” *Phys. Rev. A* **85**, 032119 (2012).

[34] S. Pironio, J.-D. Bancal, and V. Scarani, “Extremal correlations of the tripartite no-signaling polytope,” *J. Phys. A* **44**, 065303 (2011).

[35] N. D. Mermin, “Quantum mysteries revisited,” *Amer. J. Phys.* **58**, 731 (1990).

[36] G. Svetlichny, “Distinguishing three-body from two-body nonseparability by a Bell-type inequality,” *Phys. Rev. D* **35**, 3066 (1987).

[37] J. Barrett, N. Linden, S. Massar, S. Pironio, S. Popescu, and D. Roberts, “Nonlocal correlations as an information-theoretic resource,” *Phys. Rev. A* **71**, 022101 (2005).

[38] M. Navascués, E. Wolfe, D. Rosset, and A. Pozas-Kerstjens, “Genuine Multipartite Network Entanglement,” [arXiv:2002.02773](https://arxiv.org/abs/2002.02773) (2020).

[39] D. Schmid, T. C. Fraser, R. Kunjwal, A. B. Sainz, E. Wolfe, and R. W. Spekkens, “Why standard entanglement theory is inappropriate for the study of Bell scenarios,” [arXiv:2004.09194](https://arxiv.org/abs/2004.09194) (2020).

[40] E. G. Cavalcanti and R. Lal, “On modifications of Reichenbach’s principle of common cause in light of Bell’s theorem,” *J. Phys. A* **47**, 424018 (2014).

[41] J.-M. A. Allen, J. Barrett, D. C. Horsman, C. M. Lee, and R. W. Spekkens, “Quantum common causes and quantum causal models,” *Phys. Rev. X* **7**, 031021 (2017).

[42] D. Janzing, D. Balduzzi, M. Grosse-Wentrup, and B. Schölkopf, “Quantifying causal influences,” *Ann. Statist.* **41**, 2324 (2013).

[43] C. H. Miles, P. Kanki, S. Meloni, and E. J. Tchetgen Tchetgen, “On partial identification of the pure direct effect,” [arXiv:1509.01652](https://arxiv.org/abs/1509.01652) (2015).

[44] D. Malinsky, I. Shpitser, and T. Richardson, “A potential outcomes calculus for identifying conditional path-specific effects,” [arXiv:1903.03662](https://arxiv.org/abs/1903.03662) (2019).

[45] R. Bhattacharya, R. Nabi, and I. Shpitser, “Semiparametric inference for causal effects in graphical models with hidden variables,” [arXiv:2003.12659](https://arxiv.org/abs/2003.12659) (2020).

[46] I. Shpitser and E. Tchetgen Tchetgen, “Causal inference with a graphical hierarchy of interventions,” *Ann. Statist.* **44**, 2433 (2016).

[47] I. Shpitser and E. Sherman, “Identification of personalized effects associated with causal pathways,” in *Uncertainty in Artificial Intelligence*, Vol. 2018 (2018).

[48] M. J. Stensrud, J. G. Young, V. Didelez, J. M. Robins, and M. A. Hernán, “Separable effects for causal inference in the presence of competing events,” [arXiv:1901.09472](https://arxiv.org/abs/1901.09472) (2019).

[49] Z. Cai, M. Kuroki, J. Pearl, and J. Tian, “Bounds on direct effects in the presence of confounded intermediate variables,” *Biometrics* **64**, 695 (2007).

[50] C. Kang and J. Tian, “Inequality constraints in causal models with hidden variables,” in *Uncertainty in Artificial Intelligence* (2006).

[51] R. Chaves, G. Carvacho, I. Agresti, V. Di Giulio, L. Aolita, S. Giacomini, and F. Sciarrino, “Quantum violation of an instrumental test,” *Nat. Phys.* **14**, 291 (2017).

- [52] J. Bowles, F. Baccari, and A. Salavrakos, “Bounding sets of sequential quantum correlations and device-independent randomness certification,” [arXiv:1911.11056](https://arxiv.org/abs/1911.11056) (2019).
- [53] T. Moroder, J.-D. Bancal, Y.-C. Liang, M. Hofmann, and O. Guhne, “Device-independent entanglement quantification and related applications,” *Phys. Rev. Lett.* **111**, 030501 (2013).

Appendix A: Non-Commutative Polynomial Optimization

A generic NPO problem can be cast as

$$p^* = \min_{(\mathcal{H}, X, \rho)} \langle p(X) \rangle_{\rho}$$

such that $q_i(X) \succeq 0 \quad \forall i = 1 \dots m_q$,

that is, finding a Hilbert space \mathcal{H} , a positive-semidefinite operator $\rho: \mathcal{H} \rightarrow \mathcal{H}$ with trace one, and a list of bounded operators $X = (X_1 \dots X_n)$ in \mathcal{H} (where $X_i X_j \neq X_j X_i$ in general) that minimize the expectation value $\langle p(X) \rangle_{\rho} = \text{Tr}[\rho \cdot p(X)]$ of the polynomial operator $p(X)$ given some polynomial constraints $q_i(X) \succeq 0$, where $q_i(X) \succeq 0$ means that the operator $q_i(X)$ should be positive semidefinite. One can also add to the optimization statistical constraints of the form $\langle r_j(X) \rangle_{\rho} \geq 0$, for $j = 1, \dots, m_r$. Note that the NPO formalism can also accommodate equality constraints of the form $q(X) = 0$ or $\langle r_j(X) \rangle_{\rho} = 0$, since they are equivalent to the constraints $q(X), -q(X) \succeq 0$ and $\langle r_j(X) \rangle_{\rho}, \langle -r_j(X) \rangle_{\rho} \geq 0$, respectively.

The procedure for solving these problems is described in Ref. [20], and uses a hierarchy of relaxations where each of the hierarchy’s steps is an SDP instance. The solutions to these problems form a monotonically increasing sequence of lower bounds on the global minimum p^* :

$$p_1 \leq p_2 \leq \dots \leq p_{\infty} \leq p^*.$$

If the constraints $\{q_i(X) \succeq 0\}_i$ imply (explicitly or implicitly, see Ref. [20]) that all non-commuting variables X_1, \dots, X_n are bounded (and they do so in all the NPO problems considered in this work), then the sequence of lower bounds is asymptotically convergent. That is, $p_{\infty} = p^*$.

In our case, given some observed correlations, we deal with a feasibility problem about the existence of a quantum state and measurements subject to polynomial operator and statistical constraints arising from the causal networks and the observed correlations. This feasibility problem can be mapped into an optimization problem in different ways. For instance, while not being the most practical procedure, the easiest way of doing it is by considering a constant polynomial $p(X) = 1$ as the function to be optimized. This problem has solution equal to 1 provided that the polynomial and statistical

constraints are simultaneously satisfiable. Any step in the hierarchy is therefore a necessary SDP test to be satisfied for the causal model to be compatible with the observed correlations. Note that the same formalism can be used to optimize polynomials of the operators, such as, for instance, Bell-like inequalities, over quantum correlations compatible with a given causal structure [39].

Appendix B: Monomial Sets for NPO Problems

The hierarchies of semidefinite programs that bound the solutions of NPO problems can be described in terms of sets of products of the non-commutative operators in the problem. In this article we use two different hierarchies, that are both asymptotically complete. The levels in the first hierarchy are known as **NPA levels** [21, 22]. The NPA level n , \mathcal{S}_n , is associated to the set of all products of operators in the problem, of length no larger than n . For example, the set \mathcal{S}_2 associated to the inflations of the quantum triangle scenario discussed in the main text is

$$\mathcal{S}_2 = \{\mathbb{1}\} \cup \{H_p^{i,j}\}_{p,i,j} \cup \{H_p^{i,j}(H')_q^{k,l}\}_{p,q,i,j,k,l},$$

where $H, H' = E, F, G$. On the other hand, some problems may achieve tighter results at lower levels if one instead considers **local levels** [53]. The local level n , \mathcal{L}_n , is built from the products of operators that contain at most n operators of a same party. For instance, in the quantum triangle scenario, the set \mathcal{L}_1 associated to its inflations is

$$\mathcal{L}_1 = \{\mathbb{1}\} \cup \{H_p^{i,j}\}_{p,i,j} \cup \{H_p^{i,j}(H')_q^{k,l}\}_{p,q,i,j,k,l} \cup \{E_a^{i,j} F_b^{k,l} G_c^{m,n}\}_{a,b,c,i,j,k,l,m,n},$$

where $H \neq H'$. While both hierarchies are asymptotically complete, they satisfy the relation $\mathcal{S}_n \subset \mathcal{L}_n \not\subset \mathcal{S}_{n+1}$ (in fact, the smallest set of the NPA hierarchy that contains \mathcal{L}_n is \mathcal{S}_{pn} , where p is the number of parties), and thus the use of finite levels of one or the other hierarchy may vary with the specific problem to solve.

Appendix C: The treatment of latent variables with latent parents

The study of network form quantum causal structures with quantum inflation is, essentially, solving the problem of *classifying entanglement networks* in a device-independent manner [38, 39]. Generalizing to latent nonexogenous scenarios can thus be seen as a further generalization of the problem of classification of entanglement generation in general causal structures. Consider, for instance, four parties and two three-way sources of entanglement. One can imagine two distinct ways to generate the final 4-partite quantum state from the initial pair of sources. In the first case, depicted

in Fig. 10(a), each of the four parties applies arbitrary (local) quantum channels to the states they receive from the sources. In the second case, depicted in Fig. 10(b), a nonlocal quantum channel spanning Bob and Charlie’s systems is applied prior to the final assignment of Hilbert spaces to parties. Naively one might think that this further generality doesn’t add much—after all, Bob and Charlie can share arbitrary entanglement in either scenario—but that is not the case. Only the causal structure depicted in Fig. 10(b) can give rise to the state

$$\rho_{10(b)} := \frac{|AB00\rangle\langle AB00| + |A0C1\rangle\langle A0C1|}{2}, \quad (C1)$$

$$\text{where } |AB00\rangle = \frac{|0000\rangle + |1100\rangle}{\sqrt{2}}$$

and $|A0C1\rangle = \frac{|0001\rangle + |1011\rangle}{\sqrt{2}}$.

$\rho_{10(b)}$ describes maximal A – B entanglement and $C=|0\rangle$ when $D=|0\rangle$ mixed with maximal A – C entanglement and $B=|0\rangle$ when $D=|1\rangle$. Here, measuring ρ'_D in the computational basis will steer the ρ'_{ABC} towards either maximal entanglement between A and B or maximal entanglement between C and D . This is only possible if the B – C entanglement structure is determined by a node which shares causal ancestry with A as well with D . There is no node in Fig. 10(a) that satisfies these requirements, which implies that the state $\rho_{10(b)}$ cannot be generated by such a causal structure. On the other hand, ρ_{BC} in Fig. 10(b) is a node which does satisfy the requirements, and thus, both structures are not equivalent.

Alternatively, this can also be understood through monogamy of nonlocality: access to $\rho_{10(b)}$ enables maximally violating the CHSH inequality for either players A and B or by players A and C , where nonlocal parties are flagged by the value of a measurement on ρ'_D . This precisely replicates the example in Fig. 4, except that the switch setting S in Fig. 4(a) is replaced by measurement on ρ'_D in Fig. 10(b) in the computational basis.

An explicit realization of $\rho_{10(b)}$ in Fig. 10(b) is as follows. Let $\rho_{ABC} = (|00\rangle + |11\rangle)_{AB_1}$ and $\rho_{BCD} = (|00\rangle + |11\rangle)_{B_2D} \otimes |0\rangle_C$. Then, perform a controlled swap on qubits B_2 and C depending on B_1 ’s computational basis value, and trace out the subsystem B_1 .

In Sec. IV B we prescribed encoding all quantum

channels in the causal structure as unspecified unitaries that can be incorporated into the generating monomials. Though Fig. 4 there illustrated classically controlled quantum channels, uncontrolled quantum channels can equally well be incorporated into the elementary monomials. Consider applying quantum inflation to Fig. 10. Inflation imbues every unitary with a pair of indices corresponding to which copies of the root quantum states the given unitary pertains to. For the unrestricted case in Fig. 10(a), we find that misaligning the copy index pertaining to one of the root quantum states leads to

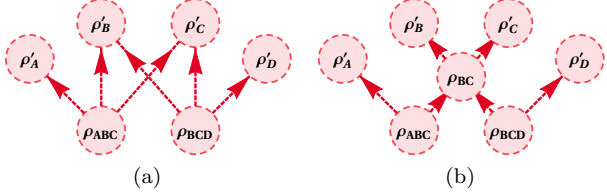


FIG. 10. Inequivalent state generating procedures. (a) depicts a two-layer state generating procedure, whereas (b) allows for the application of an arbitrary Bob-Charlie channel, generating the intermediate state ρ_{BC} , prior to distributing Hilbert spaces to the four parties. One can confirm that (a) generates a strict subset of the states realizable in (b), and quantum inflation can distinguish these two scenarios in a device-independent manner.

a pair of operators which need not commute, namely,

$$U_{BC}^{i,j} \cdot U_{BC}^{i,k} \neq U_{BC}^{i,k} \cdot U_{BC}^{i,j} \quad \text{for } j \neq k. \quad (C2)$$

On the other hand, the local unitaries relevant to Fig. 10(b) *do* commute even in the presence of misaligned copy indices, namely

$$U_B^{i,j} \cdot U_C^{i,k} = U_C^{i,k} \cdot U_B^{i,j} \quad \text{for } j \neq k. \quad (C3)$$

One can readily see, therefore, how inflation levels $n \geq 2$ give rise to SDPs with *more constrained* moment matrices when quantum inflation is applied to Fig. 10(a) instead of Fig. 10(b). This is an example of a device-independent distinction afforded by the prescription of Sec. IV B which cannot be recovered using the sequential measurements framework of Ref. [52].